nature nanotechnology

ARTICLES

https://doi.org/10.1038/s41565-021-01034-8

Check for updates

Soft-lock drawing of super-aligned carbon nanotube bundles for nanometre electrical contacts

Yunfan Guo[1,2,13], Enzheng Shi[3,4,5,13]✉, Jiadi Zhu[1,13], Pin-Chun Shen[1,6], Jiangtao Wang[1], Yuxuan Lin[1], Yunwei Mao[7], Shibin Deng[8], Baini Li[3], Ji-Hoon Park[1], Ang-Yu Lu[1], Shuchen Zhang[9], Qingqing Ji[1], Zhe Li[10], Chenguang Qiu[11], Song Qiu[12], Qingwen Li[12], Letian Dou[5], Yue Wu[10], Jin Zhang[9], Tomás Palacios[1]✉, Anyuan Cao[4]✉ and Jing Kong[1]✉

The assembly of single-walled carbon nanotubes (CNTs) into high-density horizontal arrays is strongly desired for practical applications, but challenges remain despite myriads of research efforts. Herein, we developed a non-destructive soft-lock drawing method to achieve ultraclean single-walled CNT arrays with a very high degree of alignment (angle standard deviation of ~0.03°). These arrays contained a large portion of nanometre-sized CNT bundles, yielding a high packing density (~400 μm^{-1}) and high current carrying capacity (~1.8×10^8 A cm^{-2}). This alignment strategy can be generally extended to diverse substrates or sources of raw single-walled CNTs. Significantly, the assembled CNT bundles were used as nanometre electrical contacts of high-density monolayer molybdenum disulfide (MoS_2) transistors, exhibiting high current density (~38 μA μm^{-1}), low contact resistance (~1.6 kΩ μm), excellent device-to-device uniformity and highly reduced device areas (0.06 μm^2 per device), demonstrating their potential for future electronic devices and advanced integration technologies.

Implementation of individual semiconducting carbon nanotubes (CNTs) as transistor channels and individual metallic CNTs as gate electrodes in field-effect transistors (FETs) has the potential to promote transistor miniaturization, far superior to the state-of-the-art commercial channel and gate lengths[1–4]. The van der Waals interaction between parallel nanotubes leads to the formation of bundles with high packing density and reduced transport resistance. Compared to conventional metals, metallic bundles are ideal candidates for next-generation microelectronic interconnects or wiring given the strong C–C covalent bonds that resist electromigration as well as high electrical and thermal conductivities[5]. In addition, metallic CNT bundles possess excellent mechanical (tensile strength ~80 GPa) and current carrying capacity (ampacity)[6,7].

Despite the development of numerous alignment and assembly methods for CNTs, controllable formation of highly aligned arrays of CNT bundles has not been realized. Horizontally aligned CNT arrays can be directly synthesized by chemical vapour deposition (CVD)[8], but the yield and density of aligned CNTs remain low. Outside of CVD, efforts have been focused on using solution processing to achieve aligned CNTs from random CNTs, including 'bubble-blowing', slow vacuum infiltration, solid-state drawing and domino pushing from vertically aligned multi-walled carbon nanotube (MWCNT) forests, Langmuir–Schaefer methods, DNA-assisted alignment and dimension-limited self-alignment[9–20]. Although these methods can effectively transform randomly oriented CNTs into relatively aligned CNTs, the increased density of defects and impurities (such as surfactants), barely satisfactory alignment and short length of CNTs (generally <10 μm) make it difficult to achieve aligned CNT bundles with remarkable mechanical and electrical properties.

Soft-lock drawing of super-aligned CNT bundles

We report a soft-lock drawing method to align random single-walled carbon nanotube (SWNT) networks into high-density and ultraclean super-aligned CNT arrays free of any surfactants (Fig. 1a). We first transferred CVD synthesized CNT networks[21] onto target silicon dioxide/silicon (SiO_2/Si) substrates and placed a rigid razor blade (wrapped in a nylon membrane) in contact with the CNT networks. To reduce the axial resistance force between CNTs and the substrate, the membrane was wetted with a trace small amount of volatile solvent such as ethanol or methanol. The 'soft' wetted nylon membrane ensured the effective transmission of the drawing force to all the underneath random CNTs, serving as a soft lock to fix the CNTs onto the moving blade. During the drawing process, the solvent at the CNT–substrate interface gradually evaporates. By the end of the alignment process, the CNTs are in close contact with the substrate again, leading to the recovery of the relatively large resistance between CNTs and the substrate, thereby fixing the aligned CNT arrays on the substrate tightly, and avoiding the retraction of the aligned CNTs after the tensile force was withdrawn. Supplementary Fig. 1 clearly shows the effect of the solvent: the CNT alignment assisted with an ethanol-wetted membrane has a much better result

[1]Department of Electrical Engineering and Computer Science, Massachusetts Institute of Technology, Cambridge, MA, USA. [2]Research Institute of Frontier Technology, College of Micro-Nano Electronics, Zhejiang University, Hangzhou, China. [3]Key Laboratory of 3D Micro/Nano Fabrication and Characterization of Zhejiang Province, School of Engineering, Westlake University, Hangzhou, China. [4]School of Materials Science and Engineering, Peking University, Beijing, China. [5]Davidson School of Chemical Engineering, Purdue University, West Lafayette, IN, USA. [6]Taiwan Semiconductor Manufacturing Company (TSMC), Hsinchu, Taiwan. [7]Department of Mechanical Engineering, Massachusetts Institute of Technology, Cambridge, MA, USA. [8]Department of Chemistry, Purdue University, West Lafayette, IN, USA. [9]College of Chemistry and Molecular Engineering, Peking University, Beijing, China. [10]Department of Chemical and Biological Engineering, Iowa State University, Ames, IA, USA. [11]Key Laboratory for the Physics and Chemistry of Nanodevices and Department of Electronics, Peking University, Beijing, China. [12]Division of Advanced Nano-Materials, Suzhou Institute of Nano-Tech and Nano-Bionics, Chinese Academy of Sciences, Suzhou, China. [13]These authors contributed equally: Yunfan Guo, Enzheng Shi, Jiadi Zhu. ✉e-mail: shienzheng@westlake.edu.cn; tpalacios@mit.edu; anyuan@pku.edu.cn; jingkong@mit.edu

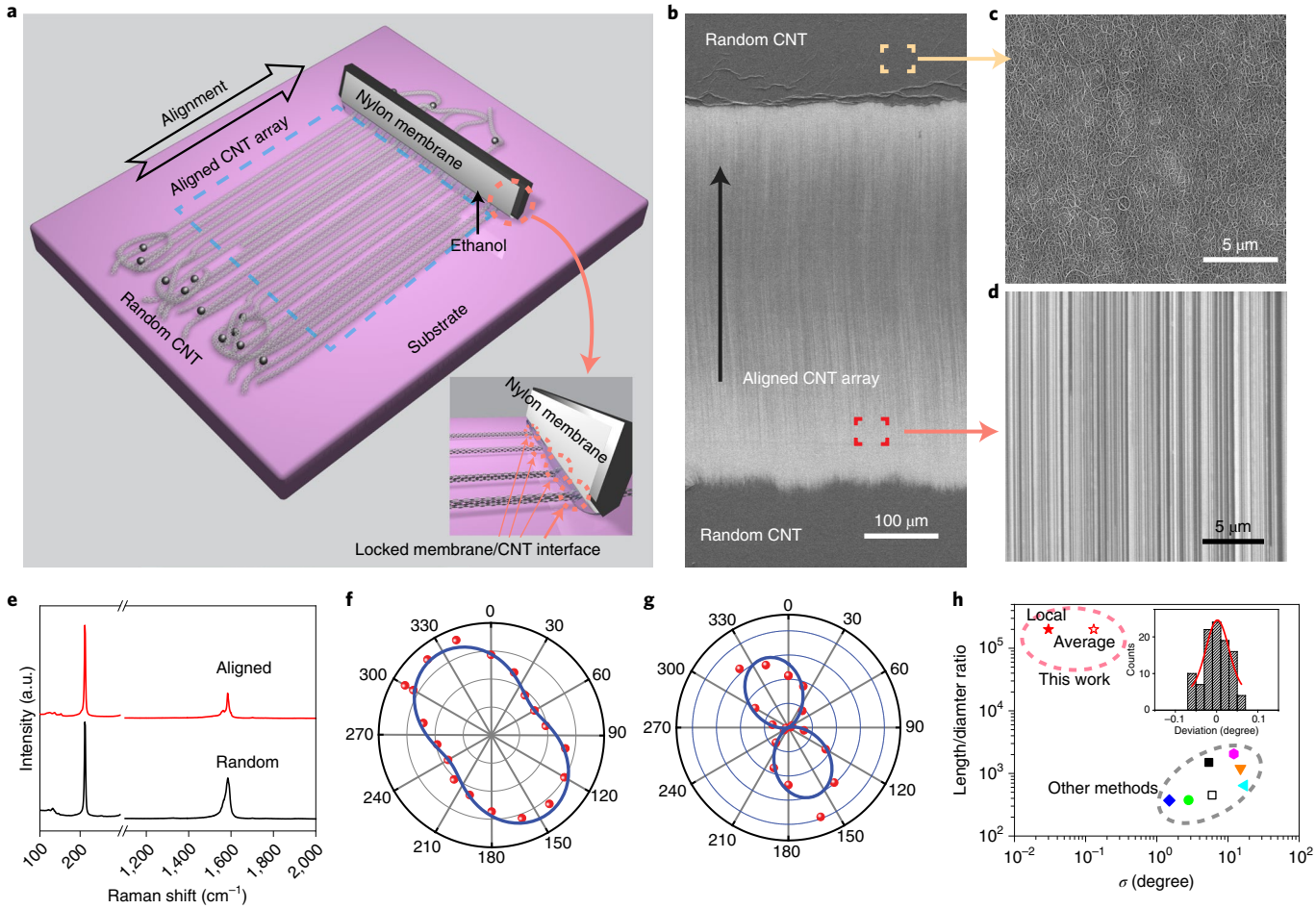

Fig. 1 | Characterizations of aligned CNT arrays created with a soft-lock drawing method. a, Schematic illustration of the soft-lock drawing alignment process from random CNTs to horizontally aligned CNT arrays. Inset, the locked interface between the soft nylon membrane and CNTs. The black solid balls represent impurities within the random CNT networks. **b**, Low-magnification SEM image of CNT arrays aligned from random CNT networks. The solid arrow indicates the alignment direction. **c**,**d**, High-magnification SEM images of random (**c**) and aligned (**d**) CNTs, respectively. **e**, Raman spectra of CNTs before (black plot, random) and after alignment (red plot, aligned). **f**,**g**, Polar plots of the fitted peak intensities of the G band as a function of sample rotation angle θ (degrees) under parallel-polarization configurations for random CNT networks (**f**), and aligned CNTs (**g**). The intensity of these two plots is centred at zero. **h**, Comparison of CNT alignment between our work with other alignment methods. The *x* axis denotes the angle s.d. (σ) of the aligned CNTs; and the *y* axis denotes the length/diameter ratio of the raw CNTs. Inset, histogram of angular distribution of aligned CNTs in **d**. $\sigma = \sqrt{\frac{\sum_{i=1}^{N}(\theta_i-\bar{\theta})^2}{N}}$, θ_i is the angle between a specific CNT and a fixed axis, and $\bar{\theta}$ is the mean angle; N is the number of CNTs for statistics. a.u., arbitrary units.

than that without any solvent. With the unidirectional drawing of the blade, the underneath CNTs moved simultaneously and eventually aligned to the drawing direction. Different from the nanoscale combing alignment of rigid nanowires[22], here the pressure is only applied at the head point of random CNTs. Moreover, a larger pressure is essential to ensure the efficient transmission of the drawing force to each of the manipulated CNTs (Supplementary Fig. 2).

As shown in the low-magnification scanning electron microscopy (SEM) image (Fig. 1b), the CNTs were aligned throughout the drawing region. After the alignment, the change of CNT orientation is obviously distinguished from the morphology images in Fig. 1c, d. Compared with the Raman spectra of the raw CNTs (Fig. 1e), the radial breathing mode and G band of aligned CNTs remain strong and sharp, and defect peaks are still negligible, indicating that this process is non-destructive.

Polarized Raman spectroscopy (excitation wavelength of 514 nm) was used to characterize the orientation difference between random CNT networks (Fig. 1f) and aligned CNT arrays (Fig. 1g). For random CNT networks obtained from floating-catalyst CVD, there is a slight pre-alignment due to the airflow during synthesis, leading to a relatively higher intensity of G band with the polarization parallel to the direction of the airflow. In comparison, for the aligned ones, the maximum intensity of G band occurred with the polarization parallel to the direction of the arrays, while the minimum intensity occurred with the polarization perpendicular to the alignment. The minimum intensity was near the background value, indicating there is almost no resonance between the incident laser and the CNTs along the direction perpendicular to the alignment. Moreover, the soft-lock drawing aligned CNT array exhibits a comparable high degree of arrangement to that of lattice-orientated growth (Supplementary Fig. 3), suggesting the outstanding alignment of CNTs from our soft-lock drawing method.

As quantified by the angular s.d. σ and the length/diameter ratio (Fig. 1h), the soft-lock drawing method exhibited a much higher

degree of alignment comparable to previously reported alignment methods, where the raw CNTs have a length of <10 μm and a length/diameter ratio <5,000 (refs. [11–16]). In comparison, our method aligned long CNTs (300 μm to ~1 mm) with a length/diameter ratio >200,000, which is imperative to preserve the excellent electronic and mechanical properties of CNTs over a longer distance, offering wider space for its potential applications. In addition, our CNTs were highly aligned with an angular s.d. σ of 0.03° (locally, based on the CNT alignment in Fig. 1d, 25 μm by 22 μm) and 0.13° (averaged from four selected regions, each 25 μm by 18 μm) from a 0.15 mm by 4.2 mm region (Supplementary Fig. 4), which is over one order of magnitude smaller than the best result from previous works ($\sim\sigma > 1.5°$, statistics are listed in Supplementary Table 1, and the σ difference between all alignment methods is compared in Fig. 1h). On the other hand, these aligned CNT arrays can be easily manipulated through polymethylmethacrylate (PMMA)-assisted transfer. As shown in Supplementary Fig. 5, CNT crosses with arbitrary stacking angles are fabricated by stacking two layers of aligned CNTs, which is promising to replace the metal interconnects inside integrated circuits and for flexible electronics applications. In addition, this soft-lock drawing method is compatible with many commonly used industrial substrates, such as polished SiO_2/Si, sapphire, glass and rough SiO_2/Si substrates (Supplementary Fig. 6a–d). Furthermore, diverse sources of random CNTs, such as commercially available SWNT fragments, (6, 5) rich SWNT powders and Bucky paper could be well aligned with the soft-lock drawing method (Supplementary Fig. 6e–g).

Mechanism of the soft-lock drawing method

To understand the mechanism of the soft-lock drawing method, we propose a flexible 'gluttonous snake' model to depict the alignment process (Fig. 2a,b; see details in Supplementary Information). As both the length of the CNT and the curvature radius (R) of the CNT moving path are much larger than its diameter, the CNT is considered as a flexible string during the alignment. In general, as the drawing force F is not exactly along the initial axial direction of CNT at the head point, there is a large component of force in the radial direction; hence the head portion of CNT will slide first and then follow a path dictated from A to B, which is defined as path A–B (Fig. 2b). After passing path A–B, the CNT will become completely aligned. The projection from path A–B to the alignment direction is defined as the alignment distance s. From our calculation, path A–B is a logarithmic spiral. The alignment distance s is expressed as:

$$s = r_0\left(\cos\alpha - e^{b\phi}\cos(\phi+\alpha)\right) \quad (1)$$

where ϕ represents the angle between the alignment direction and the axial direction at point A, which mainly depends on the initial orientation of the CNTs. The definition of r_0, α and b can be found in the Supplementary Information, and s is a measurable parameter from SEM images, which is measured to be 3 ± 0.6 μm for 10 selected CNTs when $\phi = 105°$(Supplementary Fig. 7).

For the rest of the CNTs, when the following equation (2) is satisfied, every portion of the CNT will follow the moving path of its front neighbouring portion without any radial sliding during the alignment process:

$$f_a L \le F \le \min_{0\le l\le L}\left\{\frac{L}{L-l}\left(f_r R(l) + \rho v^2\right)\right\} \quad (2)$$

where F refers to the drawing force applied to this CNT; f_r and f_a refer to the radial and axial resistance force on the CNT per unit length, respectively; ρ is the linear density of CNTs; v represents the axial velocity; l (or L) is the CNT length between the head point and the selected region (or the end).

For entangled CNT networks, the entanglement will increase the radial resistance force of the CNT significantly, but have little impact on the axial resistance force, thereby facilitating the 'gluttonous snake' alignment of the CNTs in practical circumstances. Notably, the rationality of the 'gluttonous snake' model is evidenced by the experimental results. When we intentionally shifted the direction of applied force following a wavy path, the aligned CNTs also followed a wavy path smoothly (Fig. 2c and Supplementary Fig. 8a-d), which could be useful for the fabrication of on-chip nanoscale inductors with extremely reduced area (Supplementary Fig. 8e). In addition, the alignment path can be clearly tracked. From the SEM image in Fig. 2d, the aligning path from point no. 1 to point no. 5 records the whole alignment process, and the CNTs from point no. 2 to point no. 4 can be considered as the intermediate alignment states. Based on the above discussion, our alignment process and mechanism are distinctly different from previous reports, for example, the solid-state MWCNTs alignment[10], in which an external drawing force is applied to extract the intrinsically aligned MWCNTs in one direction to produce oriented, free-standing MWCNT sheets.

Statistics of super-aligned CNT bundles

For the purpose of high-performance electronics, aligned CNTs are desired in high packing density[9,23]. During our soft-lock drawing alignment process, aligned CNTs may spontaneously form bundles when the local density of CNTs is high. We directly validated the formation of these bundles by transmission electron microscopy (TEM) (Fig. 2e and Supplementary Fig. 9), which showed CNT bundles with a width from 5 to 50 nm. Due to the presence of nano bundles, the density of soft-lock drawing aligned CNTs could not be directly determined from SEM and atomic force microscopy (AFM) imaging. Instead, optical reflective contrast of CNTs (inset of Fig. 2f) was used to calculate the line density of a CNT array[24–26]. As the average diameter of the CNTs was calculated to be 1.41 nm based on the statistics from Raman spectra (Supplementary Fig. 10), a high CNT density of approximately 400 μm^{-1} was achieved (Fig. 2f). Furthermore, we performed a statistical analysis to investigate the spatial dependence of another typical set of CNT bundles. From AFM characterizations (Fig. 2g and Supplementary Fig. 11), the density and ratio of aligned CNT bundles (we assume the aligned CNTs with a height >2 nm are bundles) showed strong dependence on the distance (L) away from the interface between the random and aligned regions. Aligned CNT bundles dominated the region when $L = 0$, with high bundle density (>8 μm^{-1}) and high bundle percentage (>80%). With increasing L to more than 300 μm, the density of aligned CNT bundles decreased down to <1 μm^{-1}. When $L > 500$ μm, there were no CNT bundles observed, indicating that the bundling CNTs gradually vanished and all remaining CNTs were individually aligned. The microscale non-uniformity of the CNT bundle is speculated to originate from the spatial distribution of pristine raw CNTs (Supplementary Figs. 12 and 13). By utilizing thicker CNT films with reduced inhomogeneity, the uniformity of aligned CNT bundles could apparently be improved.

Cleaning and long-range ordering of super-aligned CNT bundles

An additional benefit of the soft-lock drawing method is the removal of surface contamination, such as amorphous carbon and catalysts, from raw CNTs after alignment. From the TEM and SEM images (Fig. 3a), the random CNTs were initially coated with a thick amorphous sheath, but this was detached after the alignment. The effective removal of these impurities could also be observed from the AFM characterizations (Supplementary Fig. 14). As impurities interacted weakly with the CNTs, when the CNTs were pulled out from the random networks, they gradually aligned and fully contacted the substrate, whereas the impurities remained on the random CNT networks or the substrate. The remaining networks and

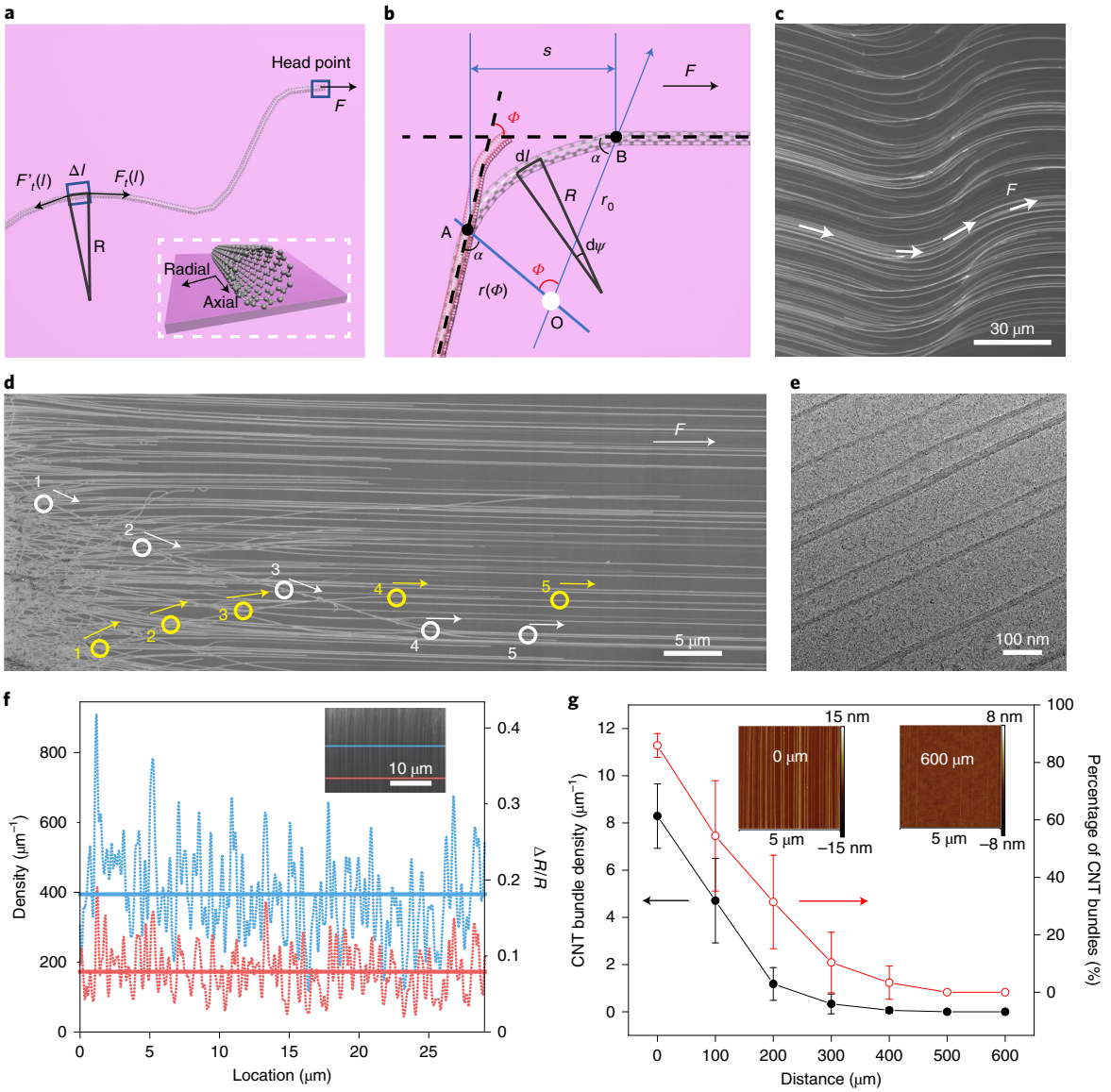

Fig. 2 | Mechanism and statistics of CNT alignment. a,**b**, Schematic illustration of 'gluttonous snake' model for CNT alignment. **a**, Force analysis of an arbitrary portion (Δl) within the flexible CNT. Inset, the definition of radial and axial directions. $F_t(l)$ is defined as the tension force at position l, which is along the axial direction of the CNT and towards the moving direction, and $F_{t'}(l)$ is defined as the tension force at position l, which is along the axial direction of the CNT but opposite to the moving direction. **b**, Logarithmic spiral path analysis of the head portion of the CNT during alignment. **c**, s.e.m. image of an intentionally aligned CNT array following a wavy path. The white arrows denote the direction of the drawing force, F. **d**, Tracking of CNTs aligned from random networks. The white and yellow circles denote the moving paths for two individual CNTs, and the white and yellow arrows denote the orientation of these two CNTs at different locations. **e**, TEM image of aligned CNT bundle arrays. **f**, Ultrahigh linear density of aligned CNTs determined by the optical imaging method. $\Delta R/R$ (right axis) represents optical reflection contrast and the left axis represents the linear density of aligned CNTs calculated from $\Delta R/R$. The two dashed plots (red and green) are extracted from the two corresponding lines in the inset optical image (on quartz glass), respectively. The two solid plots represent the average linear density of CNTs. **g**, Distance dependence of CNT bundle density and ratio. Inset, AFM images representing CNT arrays at the alignment-initiating region (distance is 0) and 600 μm away from the alignment-initiating region, respectively.

the substrate acted as a sticky filter to immobilize the impurities, resulting in the cleaning of aligned CNTs. The cleaning effect will extend our CNT alignment method to a variety of CNT sources.

In principle, the width of the aligned CNT area was determined by the width of the razor blade, and can be potentially scaled up through automation and machinery. With our current manual alignment, there are variations in the CNT spacing. Nevertheless, it can be envisioned that by extending the method to automatic alignment with modified blade (with a nanoscale rake-like structure), highly aligned CNTs with well controlled spacing can be achieved in the future. At present, the length was mostly determined by the intrinsic length of raw CNTs, ranging from hundreds of micrometres to one millimetre (Supplementary Fig. 15). To scale up the alignment, we used photoresist bands fabricated by photolithography as mechanical anchors. The extra anchors increased the friction between CNTs and substrates, and initiated multiple alignment regions from each anchor edge, which would potentially enable the large-scale alignment of CNTs (Fig. 3b).

Surprisingly, the aligned CNT arrays are strong enough to traverse designed trenches (2–20 μm wide and 1 μm deep), suspend

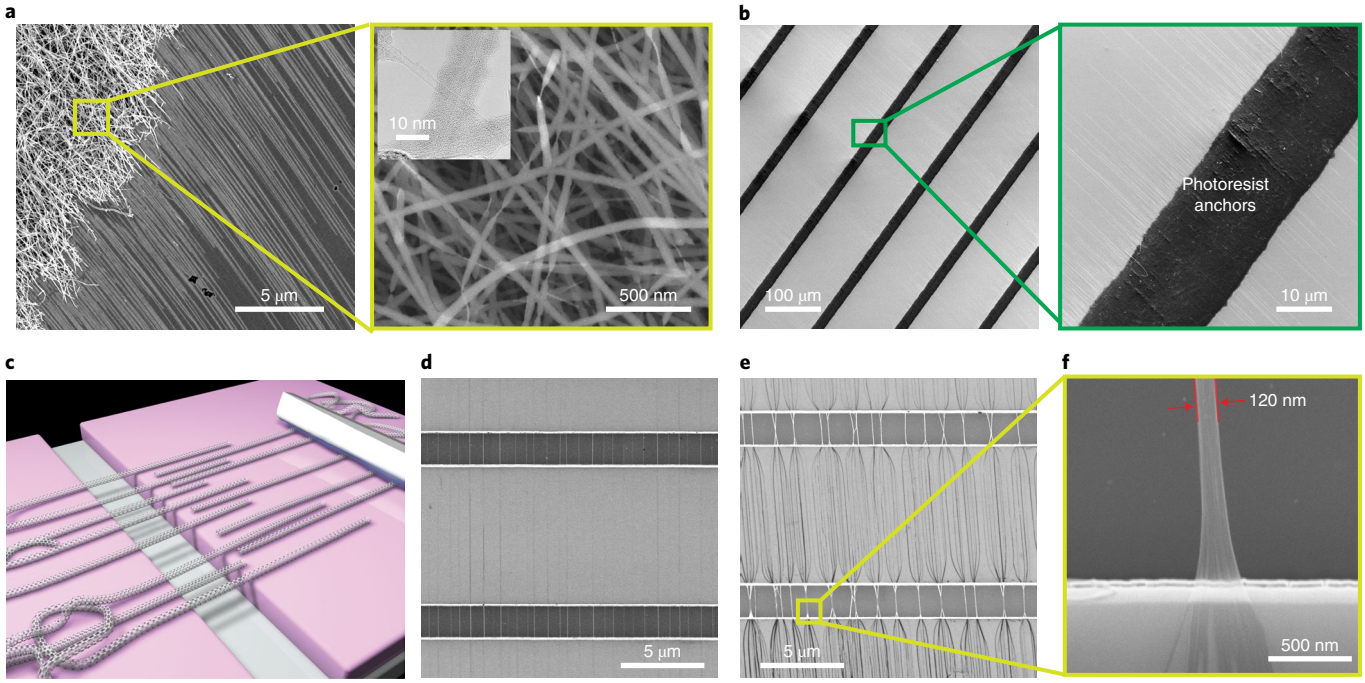

Fig. 3 | Cleaning and long-range ordering of CNTs by soft-lock drawing method. a, SEM images showing the cleaning effect from the soft-lock drawing alignment. The left SEM image shows clean, aligned CNT arrays from random CNTs coated with an amorphous carbon sheath, which is magnified in the right SEM image and inset TEM image. **b**, SEM images of large-scale aligned CNTs arrays with photoresist anchors. **c**, Schematic illustration of aligned CNT arrays across trenches. **d**, SEM image of CNT aligned arrays across 2 μm trenches. **e**, SEM image of further assembled CNT bundles. **f**, Enlarged SEM image of the selected suspended bundle in **e** with a diameter of approximately 120 nm.

themselves but keep the ordered morphologies (Fig. 3c,d and Supplementary Fig. 16). By increasing the amount of ethanol (to wet the soft membrane), adjacently aligned CNT bundles were further aggregated into a thicker bundle (up to 120 nm in diameter) when suspended across trenches (Fig. 3e,f and Supplementary Fig. 17). This is probably due to the fact that, as the solvents on the surface of nearby CNTs merge with each other, the CNTs are drawn into a bundle. When the amount of the solvent droplets on the CNTs is low and the lateral spacing between adjacent CNTs is wide, there will not be aggregation of neighbouring CNTs. However, when there is enough solvent and the neighbouring CNTs are close enough, the surface tension of ethanol will draw the adjacent CNTs to move towards each other, and finally aggregate into a thicker bundle, accompanied with the evaporation of the solvent. As the average diameter of CNTs was 1.41 nm, the number of CNTs within this bundle was estimated to be >3,000. In our work, the largest bundle suspended over the trench had a width of approximately 510 nm. Moreover, the concentrated G bands extracted from Raman mapping suggest that the strain within the bundles is uniform, which is beneficial to achieve strong CNT bundles with ultrahigh tensile strength[7].

Using aligned CNT bundles as nanometre electrical contacts

In fact, the demonstrated alignment uniformity, surface cleanness and excellent conductance of the CNT bundles already make them a promising contact material for electronic devices. Here, we made experimental demonstration of top-gated monolayer MoS_2 transistors based on CNT nanoscale contacts. Fig. 4a shows the schematic diagram of the top-gate devices. The MOCVD-grown monolayer MoS_2 film between two CNT bundles would act as the channel material once it is transferred on top of the CNT bundles. For the convenience of electrical measurement, we are also using gold (Au) probing pads to connect the CNT bundles source/drain contacts with the measurement set-ups, namely the probe station (Fig. 4b). These Au probing pads are not in touch with the MoS_2 channel and can be replaced by in-plane CNT bundles or vertical metal-filled via (Supplementary Note 1) in larger-scale integrated circuits. In these devices, the channel lengths are defined by the distance between two adjacent CNT bundles and are typically around or larger than 180 nm (Supplementary Fig. 18), while the channel width is designed as 2 μm by electron-beam lithography (EBL). As shown in Fig. 4c, 25 individual top-gated devices are fabricated in an array and cover an effective area of 25 μm × 3 μm.

In Fig. 4d, we demonstrated the transfer characteristic of 20 functional devices from the 25-device array. All these MoS_2 transistors exhibit *n*-type conduction with an on/off current ratio of approximately 10^5 and the highest on-state current being 38 μA μm^{-1}. The extracted threshold voltage (V_T) is approxmately −33 V, with a slight variation of 38.6 mV V^{-1}, demonstrating good device uniformity. The peak field-effect mobility estimated at the maximum transconductance (Supplementary Fig. 20) was approximately 3.4 cm^2 V^{-1} s^{-1}, which is comparable to the value (~3.5 cm^2 V^{-1} s^{-1}) when using Au contacts (Supplementary Fig. 21).

The outstanding linearity of the output curves (Fig. 4e) illustrates a low contact resistance of the nanoscale CNT contacts. The lowest extracted contact resistance is 1.6 kΩ μm (Fig. 4f) with an average value of approximately 2.1 kΩ μm (Supplementary Figs. 22–24 and Supplementary Table 2), which is better than most of the demonstrated metallic contact materials for MoS_2[27–31], including graphene[32], due to the absence of dangling bonds at the CNT–MoS_2 interface, and no damage is caused during the formation of the electrode as no atom or cluster bombardment process[33] is involved. Ultrahigh vacuum metal deposition[34], a phase transition in the source/drain regions[35] and using semimetal contact to reduce metal induced gap states[36] could help to provide lower contact resistance.

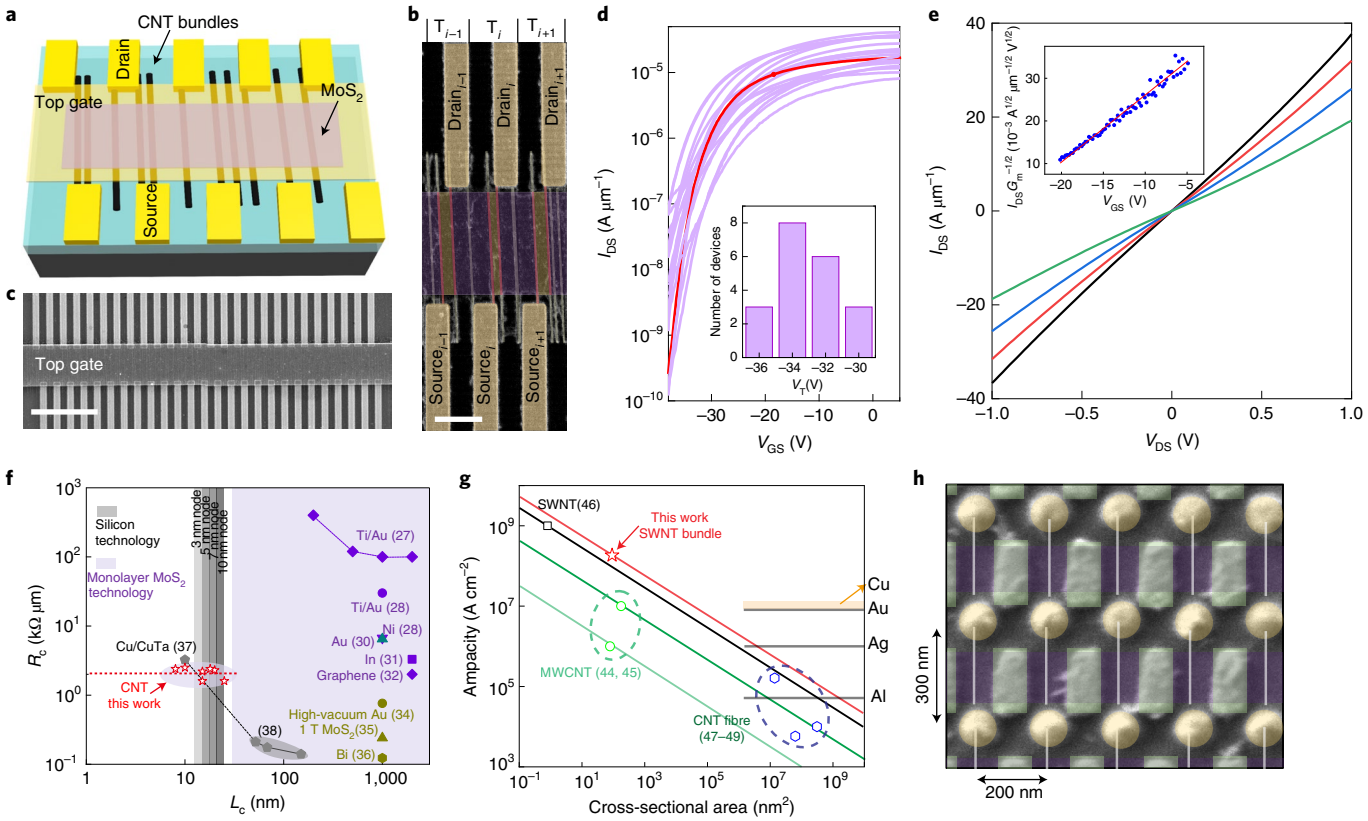

Fig. 4 | MoS_2 transistor array with CNT bundles as nanometre electrical contacts. a, Schematic diagram of the MoS_2 transistor array with top-gate design. **b**, False colour SEM image of three transistors (T_{i-1}, T_i and T_{i+1}) inside the array before the top gate and dielectric are deposited. The yellow regions are the Au probing pads. The purple rectangle is the MoS_2 with channel regions highlighted in orange. The white lines are CNT bundles with the actual source/drain parts highlighted in red. Scale bar, 1 μm. **c**, SEM image of the top-gated MoS_2 transistor array. Scale bar, 5 μm. **d**, Measured transfer characteristics of 20 MoS_2 transistors inside the array at room temperature and $V_{DS} = 1$ V. The red line demonstrates the representative performance among the 20 devices; inset, threshold voltage (V_T) distribution of the 20 devices. **e**, Measured output performance of the MoS_2 transistors; inset, channel mobility extraction. **f**, Benchmark of contact resistance (R_c) and contact length (L_c) in reported MoS_2 transistors and standard complementary metal oxide semiconductor technology. **g**, Dependence of ampacity of as-reported individual CNTs, CNT fibres and our SWNT bundle with the corresponding cross-sectional areas. The horizontal lines indicate the ampacity of conventional metals (aluminium (Al), silver (Ag), Au and copper (Cu)), and the diagonal lines indicate the correlation between ampacity and cross-sectional area based on the experimental data of individual SWNT, MWCNTs and our SWNT bundle. **h**, False colour SEM image of eight local top-gate transistors in a two-dimensional MoS_2 transistor array with single device area of 0.06 μm^2. The green rectangles are the local top gates. The orange circles are the vertical metal-filled via in contact with the CNT bundles (white lines). The purple rectangles are the monolayer MoS_2 channels. 10 nm aluminium oxide (Al_2O_3) is used as the top-gate dielectric.

However, as the feature size continues to scale down, conventional metal contacts will encounter higher resistance due to enhanced carrier scattering at metal grain boundaries and contact sidewalls as well as the increased portion of the high resistance diffusion barrier at smaller scale[37–39]. However, the CNT bundle nano electrodes do not suffer from these problems and can be scaled down even further by narrowing the width of the bundles, until reaching the diameter of an SWNT, as shown by the red dashed line in Fig. 4f, indicating it could be a promising contact technology compared with the most advanced silicon technologies[39,40] and even for the ultimate scaling of contacts. The CNT bundle also possesses much higher ampacity (~1.8×10^8 A cm^{-2}, Supplementary Fig. 25), compared with conventional metal contacts[41–43] and many other carbon-based materials[44–49], which is a significant advantage for contact dimensions scaling down (Fig. 4g).

The MoS_2 transistors with CNT bundle contacts possess advantages over silicon devices of similar channel length (Supplementary Fig. 26) in terms of device area (~0.18 μm^2, Supplementary Fig. 27) due to the highly reduced contact area. We also observed good device-to-device uniformity among different transistor arrays (Supplementary Fig. 28), demonstrating the possibility of larger-scale integration by fabricating more devices in one large array or making more transistor arrays with few devices.

Further scaling of the device area can be done by forming vertical metal-filled via at the end of the CNT bundles, which provides an even smaller device area of 0.06 μm^2 (Fig. 4h) and higher integration density. Local top-gate structure is used in these devices with 120 nm gate length to prevent the overlap between the gate and source/drain terminals and thus reduce the total gate capacitance. This method is useful to realize circuit level integration based on MoS_2 transistors with CNT bundle contact, as we experimentally demonstrated an 8×8 top-gate MoS_2 transistor array (Supplementary Fig. 29) and proposed a complete back-end-of-line (BEOL) compatible strategy (Supplementary Note 1) to realize even larger-scale integrated circuit, for example the static random access memory array (Supplementary Fig. 30), with improved control over the spacing between CNT bundles (Supplementary Note 2), which illustrates the potential for applying the CNT bundle contacts for large-scale integrated circuits with highly scaled contacts. Semiconducting CNT bundles can also be aligned, fabricated into FETs and integrated with a similar approach (Supplementary Fig. 31), which also demonstrates the promising

applications for our CNT alignment method and BEOL-compatible integration strategy.

Conclusions

In this work, we developed a non-destructive soft-lock drawing method to achieve ultraclean SWNT arrays with a very high degree of alignment, which allows both straight and wavy alignment, and works for both metallic and semiconducting CNTs. We experimentally demonstrated MoS_2 transistor arrays based on metallic CNT bundle contacts, FETs with aligned semiconducting CNT channels and hypothesized highly scaled on-chip inductors made by wavy CNT bundles. The proposed technology based on the integration of metallic and semiconducting low-dimensional nanomaterials represents a new paradigm for the fabrication of future nano-electronics. By further improving the control of the spatial location of all individual CNTs and the spacing between neighbouring CNTs, the realized clean and low-resistance CNT contact could provide a way to make nanoscale contacts for two-dimensional material or other material systems to the ultimate scaling of transistor contacts. The extremely small thickness of the CNT bundles also ensures nanometre-scale device thickness. With more optimizations, the metallic CNT bundles could be used as highly scaled source/drain electrodes of both logic and memory device in BEOL integrations or three-dimensional integrations with low-dimensional material systems.

Online content

Any methods, additional references, Nature Research reporting summaries, source data, extended data, supplementary information, acknowledgements, peer review information; details of author contributions and competing interests; and statements of data and code availability are available at https://doi.org/10.1038/s41565-021-01034-8.

Received: 16 February 2021; Accepted: 14 October 2021;
Published online: 20 January 2022

References

1. Cao, Q., Tersoff, J., Farmer, D. B., Zhu, Y. & Han, S.-J. Carbon nanotube transistors scaled to a 40-nanometer footprint. *Science* **356**, 1369–1372 (2017).
2. Desai, S. B. et al. MoS_2 transistors with 1-nanometer gate lengths. *Science* **354**, 99–102 (2016).
3. Qiu, C. et al. Scaling carbon nanotube complementary transistors to 5-nm gate lengths. *Science* **355**, 271–276 (2017).
4. Shulaker, M. M. et al. Carbon nanotube computer. *Nature* **501**, 526–530 (2013).
5. Wilson, L. *International Technology Roadmap for Semiconductors (ITRS)* (Semiconductor Industry Association, 2013).
6. Collins, P. G., Arnold, M. S. & Avouris, P. Engineering carbon nanotubes and nanotube circuits using electrical breakdown. *Science* **292**, 706–709 (2001).
7. Bai, Y. et al. Carbon nanotube bundles with tensile strength over 80 GPa. *Nat. Nanotechnol.* **13**, 589–595 (2018).
8. Zhang, R., Zhang, Y. & Wei, F. Horizontally aligned carbon nanotube arrays: growth mechanism, controlled synthesis, characterization, properties and applications. *Chem. Soc. Rev.* **46**, 3661–3715 (2017).
9. Cao, Q. et al. Arrays of single-walled carbon nanotubes with full surface coverage for high-performance electronics. *Nat. Nanotechnol.* **8**, 180–186 (2013).
10. Jiang, K., Li, Q. & Fan, S. Spinning continuous carbon nanotube yarns. *Nature* **419**, 801 (2002).
11. He, X. et al. Wafer-scale monodomain films of spontaneously aligned single-walled carbon nanotubes. *Nat. Nanotechnol.* **11**, 633–638 (2016).
12. Jinkins, K. R. et al. Nanotube alignment mechanism in floating evaporative self-assembly. *Langmuir* **33**, 13407–13414 (2017).
13. Mclean, R. S., Huang, X., Khripin, C., Jagota, A. & Zheng, M. Controlled two-dimensional pattern of spontaneously aligned carbon nanotubes. *Nano Lett.* **6**, 55–60 (2006).
14. Yu, G., Cao, A. & Lieber, C. M. Large-area blown bubble films of aligned nanowires and carbon nanotubes. *Nat. Nanotechnol.* **2**, 372–377 (2007).
15. Zhang, M. et al. Strong, transparent, multifunctional, carbon nanotube sheets. *Science* **309**, 1215–1219 (2005).
16. Li, X. et al. Langmuir–Blodgett assembly of densely aligned single-walled carbon nanotubes from bulk materials. *J. Am. Chem. Soc.* **129**, 4890–4891 (2007).
17. Wang, D., Song, P., Liu, C., Wu, W. & Fan, S. Highly oriented carbon nanotube papers made of aligned carbon nanotubes. *Nanotechnol.* **19**, 075609 (2008).
18. Sun, W. et al. Precise pitch-scaling of carbon nanotube arrays within three-dimensional DNA nanotrenches. *Science* **368**, 874–877 (2020).
19. Zhao, M. et al. DNA-directed nanofabrication of high-performance carbon nanotube field-effect transistors. *Science* **368**, 878–881 (2020).
20. Liu, L. et al. Aligned, high-density semiconducting carbon nanotube arrays for high-performance electronics. *Science* **368**, 850–856 (2020).
21. Li, Z. et al. Large area, highly transparent carbon nanotube spiderwebs for energy harvesting. *J. Mater. Chem.* **20**, 7236–7240 (2010).
22. Yao, J., Yan, H. & Lieber, C. M. A nanoscale combing technique for the large-scale assembly of highly aligned nanowires. *Nat. Nanotechnol.* **8**, 329–335 (2013).
23. Hu, Y. et al. Growth of high-density horizontally aligned SWNT arrays using Trojan catalysts. *Nat. Commun.* **6**, 6099 (2015).
24. Deng, S. et al. High-throughput determination of statistical structure information for horizontal carbon nanotube arrays by optical imaging. *Adv. Mater.* **28**, 2018–2023 (2016).
25. Liu, K. et al. Systematic determination of absolute absorption cross-section of individual carbon nanotubes. *Proc. Natl Acad. Sci. USA* **111**, 7564–7569 (2014).
26. Mak, K. F. et al. Measurement of the optical conductivity of graphene. *Phys. Rev. Lett.* **101**, 196405 (2008).
27. Liu, H. et al. Switching mechanism in single-layer molybdenum disulfide transistors: an insight into current flow across Schottky barriers. *ACS Nano.* **8**, 1031–1038 (2013).
28. Allain, A., Kang, J., Banerjee, K. & Kis, A. Electrical contacts to two-dimensional semiconductors. *Nat. Mater.* **14**, 1195–1205 (2015).
29. Guo, Y. et al. Additive manufacturing of patterned 2D semiconductor through recyclable masked growth. *Proc. Natl Acad. Sci. USA* **116**, 3437–3442 (2019).
30. Smithe, K. K., English, C. D., Suryavanshi, S. V. & Pop, E. Intrinsic electrical transport and performance projections of synthetic monolayer MoS_2 devices. *2D Mater.* **4**, 011009 (2016).
31. Wang, Y. et al. Van der Waals contacts between three-dimensional metals and two-dimensional semiconductors. *Nature* **568**, 70–74 (2019).
32. Leong, W. S. et al. Low resistance metal contacts to MoS_2 devices with nickel-etched-graphene electrodes. *ACS Nano.* **9**, 869–877 (2015).
33. Liu, Y. et al. Approaching the Schottky–Mott limit in van der Waals metal–semiconductor junctions. *Nature* **557**, 696–700 (2018).
34. English, C. D. et al. Improved contacts to MoS_2 transistors by ultra-high vacuum metal deposition. *Nano Lett.* **16**, 3824–3830 (2016).
35. Kappera, R. et al. Phase-engineered low-resistance contacts for ultrathin MoS_2 transistors. *Nat. Mater.* **13**, 1128–1134 (2014).
36. Shen, P. et al. Ultralow contact resistance between semimetal and monolayer semiconductors. *Nature* **593**, 211–217 (2021).
37. Badaroglu, M. et al. PPAC scaling enablement for 5 nm mobile SoC technology. In *Proc. 47th European Solid-State Device Conference (ESSDERC 2017)* 240–243 (IEEE, 2017).
38. Ieong, M. et al. Transistor scaling with novel materials. *Mater. Today* **9**, 26–31 (2006).
39. Naik, M. Interconnect trend for single digit nodes. In *International Electron Devices Meeting Technical Digest (IEDM)*, San Francisco, USA, 1–5 December (IEEE, 2018).
40. Yakimets, D. et al. Power aware FinFET and lateral nanosheet FET targeting for 3 nm CMOS technology. In *International Electron Devices Meeting Technical Digest (IEDM)*, San Francisco, USA, 2–6 December (IEEE, 2017).
41. Subramaniam, C. et al. One hundred fold increase in current carrying capacity in a carbon nanotube–copper composite. *Nat. Commun.* **4**, 2202 (2013).
42. Lloyd, J. & Clement, J. Electromigration in copper conductors. *Thin Solid Films* **262**, 135–141 (1995).
43. Black, J. R. Electromigration failure modes in aluminum metallization for semiconductor devices. *Proc. IEEE* **57**, 1587–1594 (1969).
44. Dai, H., Wong, E. W. & Lieber, C. M. Probing electrical transport in nanomaterials: conductivity of individual carbon nanotubes. *Science* **272**, 523–526 (1996).
45. Frank, S., Poncharal, P., Wang, Z. & De Heer, W. A. Carbon nanotube quantum resistors. *Science* **280**, 1744–1746 (1998).
46. Yao, Z., Kane, C. L. & Dekker, C. High-field electrical transport in single-wall carbon nanotubes. *Phys. Rev. Lett.* **84**, 2941 (2000).
47. Zhao, Y., Wei, J., Vajtai, R., Ajayan, P. M. & Barrera, E. V. Iodine doped carbon nanotube cables exceeding specific electrical conductivity of metals. *Sci. Rep.* **1**, 83 (2011).
48. Behabtu, N. et al. Strong, light, multifunctional fibers of carbon nanotubes with ultrahigh conductivity. *Science* **339**, 182–186 (2013).
49. Wang, X. et al. High-ampacity power cables of tightly-packed and aligned carbon nanotubes. *Adv. Func. Mater.* **24**, 3241–3249 (2014).

Methods

Synthesis of CNT networks via floating-catalyst CVD method. SWNT networks were synthesized via the floating-catalyst CVD method with ferrocene/xylene/sulfur as precursors at atmospheric pressure. Metal (such as nickel and copper) foils were placed downstream of a quartz tube to collect flowing CNT networks. First, the CVD system was heated to 1,160°C with 20 sccm of argon (Ar) gas flow (99.999% purity). Then the precursor solution containing ferrocene (0.045 g ml^{-1}) and sulfur (0.001 g ml^{-1}) in xylene was injected into the upstream side at a rate of 5 ml min^{-1}. Meanwhile, the carrier gas was switched to Ar/hydrogen (H_2) forming gas (V_{Ar}/V_{H_2} = 0.85/0.15) at a rate of 1,500 sccm. The growth time was from 5 to 60 min to grow CNT networks with controllable thickness. The as-grown CNT networks could be directly peeled off from the metal foils and then transferred to arbitrary substrates (SiO_2/Si, Si, quartz and so on).

Alignment of CNTs via soft-lock drawing. We developed a unique soft-lock drawing method to acquire horizontally aligned CNT arrays from random CNT networks. First, the random CNT networks were transferred onto target substrates. One piece of nylon membrane filter (GE Healthcare Life Sciences) wetted by a trace amount of volatile solvent (for example, ethanol, methanol, isopropyl alcohol and acetone) was used to cover a razor blade. The razor blade was then pressed against the random CNT networks. Under a unidirectional force parallel to the substrate, the alignment of CNTs occurred along the pulling direction. The soft nylon membrane acted as a buffer layer between CNTs and the razor blade, which would improve the contact between CNTs and the rigid razor blade and ensure the external force was applied on each CNT uniformly.

Transfer of aligned CNT arrays. To transfer aligned CNT arrays to TEM grids or other substrates to construct arbitrary CNT crosses, a layer of PMMA (950 PMMA A4, MICROCHEM) was spin-coated on the SiO_2/Si substrate with aligned CNT arrays. The spin-coating speed was 3,000 r.p.m. and the duration time was 1 min. Then the substrate was placed on 120 °C hot plate for 10 min to condense the PMMA. The PMMA-coated substrate was subsequently immersed into potassium hydroxide (KOH) (1 mol l^{-1}) etchant solution (90 °C for 2 h). After the PMMA/CNTs released from the substrate, it was transferred to distilled water repeatedly to remove the residual KOH. The clean PMMA/CNTs layer was transferred to the target substrate and annealed at 120 °C on a hot plate for 30 min. Finally, the PMMA layer was removed via immersion in 60 °C acetone for 30 min.

Growth of monolayer MoS_2 via the MOCVD method. The target 285 nm SiO_2/Si substrate was placed vertically inside a hot-wall tube furnace. Molybdenum hexacarbonyl (Sigma Aldrich) and diethyl sulfide (Sigma Aldrich) are used as precursors for molybdenum (Mo) and sulfur (S), respectively. Sodium chloride is placed in the upstream region of the furnace to improve the synthesis results; 100 sccm of Ar was introduced in the system as a carrier gas. The flow rates of precursors are 0.1 sccm for molybdenum hexacarbonyl, 2 sccm for diethyl sulfide, which are regulated by individual mass flow controllers. The growth system was heated to 450 °C for 18 h at approximately 6 Torr. The whole system was cooled down to room temperature after growth.

Transferring monolayer MoS_2 to CNT arrays. Polystyrene (PS, 280,000 g mol^{-1}, Sigma Aldrich) was dissolved inside toluene by 9.0 wt% and spin-coated onto as-grown monolayer MoS_2 film at 2,500 r.p.m. for 30 s. After heating at 160 °C for 15 min, the MoS_2 samples were released from the SiO_2/Si substrate by water with the method described in Gurarslan et al.[50]. The free-standing PS/MoS_2 hybrid film was easily picked up and attached onto the substrate with the prepared CNT arrays. The sample was subsequently baked at 70 °C for 15 min to remove the water residue and at 160 °C for 15 min to spread the polymer as well as to enhance the adhesion between the MoS_2 and the substrate. The whole sample was then immersed in cold toluene for 20 min to remove PS.

Semiconducting CNT solution preparation. Raw Arc-discharged SWNTs were purchased from Carbon Solution Inc. (AP-SWNTs, AP-A204). The dispersant 9-(1-octylonoyl)-9H-carbazole-2,7-diyl (PCz) were prepared by Suzuki polycondensation[51]; 10 mg PCz and 10 mg SWNTs were mixed in 10 ml of toluene. The solutions were ultrasonicated with a top-tip dispergator (Sonics VC500) for 30 min at an amplitude level of 50%, and then were centrifuged at 20,000 r.p.m. for 1 h (Allegra X-22R centrifuge) to remove most of the bundles and insoluble materials. The supernatant was collected and centifugated at 50,000 r.p.m. for 2 h. Finally, the supernatants were collected for fabrication of thin film.

Semiconducting CNT thin-film preparation. The uniform semiconducting CNT films were fabricated by the dip-coating method. The commercially purchased silica wafers were ultrasonicated for 5 min in acetone, ethanol and distilled water successively. Then the wafers were dried by stream of nitrogen (N_2) and heated at 120 °C for 30 min. The as-prepared semiconducting CNT solution was diluted five times with toluene. The substrate was immersed in the diluted solution for 20 h. Then the substrate was taken out of the solution and blowed with 99.999% N_2. Finally, the substrate with CNT film was baked at 120 °C for 60 min at atmosphere.

Device fabrication and electrical characterization. For ampacity measurement, the aligned CNT bundles on 300 nm SiO_2/Si substrate were located through SEM, and electrically contacted by 5 nm Ti/100 nm Au electrodes fabricated through EBL, electron-beam evaporation and a lift-off process.

For back-gated MoS_2 FETs, 285 nm SiO_2/Si substrates were used as the gate dielectric and electrode, respectively. A MOCVD-grown monolayer MoS_2/CNT stack was first transferred onto SiO_2/Si substrates using the afore-mentioned methods. EBL and reactive ion etching with oxygen plasma were used to define the device area of interest by removing other additional CNT bundles and MoS_2 on the substrates. EBL and electron-beam evaporation (~4×10^{-6} Torr) followed by a lift-off process were used to pattern and deposit 0.2 nm chromium (Cr)/75 nm Au stacks as the assistive electrical contacts to the CNTs.

For top-gated MoS_2 FETs with CNT contacts, starting from the back-gated devices, the sample is annealed at 250 °C for 1 h in N_2 atmosphere at 0.2 Torr to enhance the contacts and remove moisture. A 50 nm Al_2O_3 dielectric layer is then deposited onto the surface with the atomic layer deposition method. Subsequently, EBL, electron-beam evaporation and a lift-off process were carried out to pattern and deposit a 0.2 nm Cr/75 nm Au stack as the top-gate electrode.

The electrical measurements of ampacity and back-gated MoS_2 FETs were carried out in a cryogenic probe station (Lakeshore) at room temperature using a semiconductor parameter analyser (Agilent B1500A). For the measurements in vacuum, the pressure of the chamber was kept around 10^{-6} Torr.

The electrical measurements of top-gated MoS_2 FETs were carried out in atmosphere and room temperature using a semiconductor parameter analyser (Agilent 4155C).

The fabrication process for the two-dimensional MoS_2 transistor array/circuit based on CNT bundles is given in Supplementary Note 1. The electrical measurements of back-gate semiconducting CNT FETs were carried out in atmosphere and room temperature using a semiconductor parameter analyser (Agilent B1500A).

Morphology and structure characterization. The morphology and structure were characterized using Hitachi S4800 SEM, Hitachi SU8230 SEM, ZEISS GeminiSEM and Tecnai G2 F20 U-TWIN TEM. Raman spectra were recorded with a micro-Raman spectrometer (Renishaw inVia plus). An Olympus BX51 microscope with CCD (DP71), tungsten-halogen lamp and objective (×100, numerical aperture 0.9) were used for optical imaging. Optical contrasts in R, G, B channels were averaged for calculating CNT density.

For polarized spectrum characterization, a Horiba HR800 Raman system with a laser excitation of 514 nm was used to characterize the CNT film optically before and after alignment using our method. Parallel polarization was realized by rotating the polarizer. The maximum peak intensity of the G band was observed when the CNT alignment direction was along the polarization direction of the polarizer, and minimum G band intensity was observed when the polarizer was perpendicular to that direction. The minimum intensity was very close to the background signal, which is consistent with the dipole antennae model of an array of well-aligned structures. The change of the G peak's intensity indicates the direction of CNT alignment.

Data availability

All data are available in the manuscript or supplementary information. All materials and data are available on request to J.K., A.C., T.P. and E.S.

References

50. Gurarslan, A. et al. Surface-energy-assisted perfect transfer of centimeter-scale monolayer and few-layer MoS_2 films onto arbitrary substrates. *ACS Nano.* **8**, 11522 (2014).
51. Gu, J. et al. Solution-processable high-purity semiconducting SWCNTs for large-area fabrication of high-performance thin-film transistors. *Small* **12**, 4993–4999 (2016).

Acknowledgements

We thank F. Yang and Y. Li from Peking University for helpful discussions, and the Instrumentation and Service Center for Physical Sciences (ISCPS) at Westlake University for part of morphological characterizations. This work is partially supported by the Air Force Office of Scientific Research under the MURI-FATE program, grant no. FA9550-15-1-0514 (Y.G. and J.K.); NSFC 51672005 and Natural Science Foundation of Beijing 2212028 (A.C.), as well as by the US Army Research Office through the Institute for Soldier Nanotechnologies, under cooperative agreement no. W911NF-18-2-0048 (T.P., J.-D.Z., Y.L., P.-C.S., A.-Y.L. and J.K.), US Army Research Office under grant no. W911NF-18-1-0431 (J.W., J.-H.P. and J.K.), the STC Center for Integrated Quantum Materials, NSF grant no. DMR-1231319 (Q.J. and J.K.), the Center for Energy Efficient

Electronics Science (NSF Grant No. 0939514) (P.-C.S. and J.K.) and the Office of Naval Research, grant no. N00014-19-1-2296 (L.D.).

Author contributions

Y.G., E.S., J.-D.Z. and J.K. designed the study. Y.G. and E.S. performed material synthesis, characterization and CNT alignment. J.-D.Z. performed device, array fabrication and measurements. P.-C.S. performed the initial device fabrication and measurements. J.W. performed the flexible modelling of CNTs alignment. Y.M. performed the initial mechanism modelling of CNTs alignment. Y.L. performed the CNT ampacity measurement. S.D. conducted the measurement of CNT density. J.-H.P. performed the MOCVD synthesis of MoS_2. A.-Y.L. performed the statistics of CNTs diameter from Raman measurements. S.Z. conducted polarization Raman measurements. S.Q. and Q.L. provided CNT materials. B.L., Q.J., Z.L, C.Q., L.D., S.Q. Q.L., Y.W., J.Z., T.P. and A.C. participated in data analysis. E.S., Y.G. and J.-D.Z. wrote the manuscript. All authors read and revised the manuscript.

Competing interests

E.S., Y.G., B.L. and A.C. have applied for a patent related to the results presented in Figs. 1, 2f and 3a,c–f and Supplementary Figs. 1–6, 14 and 25 with patent application number 2021113134358. The other authors declare no competing interests.

Additional information

Supplementary information The online version contains supplementary material available at https://doi.org/10.1038/s41565-021-01034-8.

Correspondence and requests for materials should be addressed to Enzheng Shi, Tomás Palacios, Anyuan Cao or Jing Kong.

Peer review information *Nature Nanotechnology* thanks the anonymous reviewers for their contribution to the peer review of this work.